

Universality class of the depinning transition in the two-dimensional Ising model with quenched disorder

X. P. Qin^{1,2}, B. Zheng¹ and N. J. Zhou¹

¹ Department of Physics, Zhejiang University, Hangzhou 310027, P.R. China

² School of Science, Zhejiang University of Science and Technology, Hangzhou 310023, P.R. China

E-mail: zheng@zimp.zju.edu.cn

Abstract. With Monte Carlo methods, we investigate the universality class of the depinning transition in the two-dimensional Ising model with quenched random fields. Based on the short-time dynamic approach, we accurately determine the depinning transition field and both static and dynamic critical exponents. The critical exponents vary significantly with the form and strength of the random fields, but exhibit independence on the updating schemes of the Monte Carlo algorithm. From the roughness exponents ζ , ζ_{loc} and ζ_s , one may judge that the depinning transition of the random-field Ising model belongs to the new dynamic universality class with $\zeta \neq \zeta_{loc} \neq \zeta_s$ and $\zeta_{loc} \neq 1$. The crossover from the second-order phase transition to the first-order one is observed for the uniform distribution of the random fields, but it is not present for the Gaussian distribution.

PACS numbers: 64.60.Ht, 68.35.Rh, 05.10.Ln

1. Introduction

In recent years many activities have been devoted to the study of dynamic processes far from equilibrium. An example is the domain-wall dynamics in disordered media, which is important from both experimental and theoretical perspectives. A crucial feature of the driven domain interface in disordered media is the *depinning* phase transition at zero temperature. For the domain-wall motion in ultrathin magnetic films, the Edwards-Wilkinson equation with quenched disorder (QEW) is a typical theoretical approach [1, 2, 3, 4, 5, 6, 7, 8]. It is usually believed that different variants of the model belong to a same universality class.

The QEW equation is a phenomenological model, without detailed microscopic structures and interactions of the materials. The domain wall in a two-dimensional system is effectively described by a single-valued elastic string. An alternative, possibly more realistic approach, may be to construct lattice models at the microscopic level. The two-dimensional random-field Ising model with a driving field (DRFIM) is the simplest example [9, 10, 11, 12, 13]. In the DRFIM model, overhangs and islands may be created during the dynamic evolution, and the domain wall is not single-valued and one dimensional. The DRFIM model is closer to experiments [14, 15, 16] and does not suffer from the theoretical self-inconsistence as in the QEW equation [17]. Very recently it has been demonstrated that the DRFIM model may not belong to the universality class of the QEW equation [12, 13]. To distinguish these two models, one needs accurate measurements of the critical exponents. In this respect, the short-time dynamic approach has been proven to be efficient [5, 18, 19, 20, 21, 12, 13].

The purpose of this paper is to clarify the universality class of the DRFIM model. In Refs. [12, 13], Monte Carlo simulations are performed at a fixed strength of the random fields with a uniform distribution, i.e., $\Delta = 1.5$. In this paper, we systematically investigate the possible dependence of the critical exponents on the strength and form of the random fields, and the updating schemes of the Monte Carlo algorithm, including the crossover from the second-order transition to the first-order one. On the other hand, we measure not only the global and local roughness exponents ζ and ζ_{loc} , but also the *spectral* roughness exponent ζ_s , to identify the dynamic universality class of the domain interface. Following Ref. [22], there are four different universality classes in the interface growth, namely,

$$\begin{aligned} \text{if } \zeta_s < 1, \zeta_{loc} = \zeta_s & \begin{cases} \zeta_s = \zeta & \text{Family-Vicsek} \\ \zeta_s \neq \zeta & \text{intrinsic,} \end{cases} \\ \text{if } \zeta_s > 1, \zeta_{loc} = 1 & \begin{cases} \zeta_s = \zeta & \text{super-rough} \\ \zeta_s \neq \zeta & \text{faceted.} \end{cases} \end{aligned} \quad (1)$$

In Ref. [23], however, it suggests that there is a new universality class of *anomalous roughening*, with $\zeta \neq \zeta_{loc} \neq \zeta_s$ and $\zeta_{loc} \neq 1$. We verify that the DRFIM model belongs to such a new dynamic universality class. In section 2, the model and scaling analysis are described. In section 3, numerical results are presented. Section 4 includes the conclusions.

2. Model and scaling analysis

2.1. Model

The two-dimensional (2D) random-field Ising model with a driving field is defined by the Hamiltonian

$$\mathcal{H} = -J \sum_{\langle ij \rangle} S_i S_j - \sum_i (h_i + H) S_i. \quad (2)$$

where $S_i = \pm 1$ is an Ising spin at site i of a rectangle lattice $L_x \times L_y$, $\langle ij \rangle$ denotes a summation over nearest neighbors and H is a homogeneous driving field. The random-field h_i may be distributed in different forms. A typical example is a uniform distribution within an interval $[-\Delta, \Delta]$, following Refs. [9, 12, 13]. We take Δ from $0.8J$ to $2.3J$ and set the coupling constant $J = 1$. Another example is a Gaussian distribution with mean zero and standard deviation σ . Different form and strength of the random fields may lead to different kinds of phase transitions [24, 25]. At large Δ or σ , the depinning transition is of second-order for both the uniform and Gaussian distributions. As Δ decreases, the depinning transition crosses over to a first-order one for the uniform distribution which is bounded. However, such a crossover is not present for the Gaussian distribution which is unbounded.

We first concentrate on the uniform distribution of the random fields and the random-single-spin-flip Monte Carlo algorithm, and then extend the calculations to the Gaussian distribution and to different updating schemes. Simulations are performed at zero temperature with lattice sizes $L_y = 256, 512, 1024, \text{ and } 2048$ up to $t_{max} = 1280, 2560$ or 5120 for different random fields. Total samples for average are about 20000. Main results are presented with $L_y = 1024$ and simulations of different L_y confirm that finite-size effects are already negligibly small. L_x is taken to be sufficiently large so that the boundary is not reached. Statistical errors are estimated by dividing the total samples in a few subgroups. If the fluctuation in the time direction is comparable with or larger than the statistical error, it will be taken into account.

The initial state is a *semi-ordered* state with a perfect domain wall in the y direction. The periodic boundary condition is used in y direction, while the spins at the boundary in x direction are fixed. To eliminate the pinning effect irrelevant for disorder, we rotate the lattice such that the initial domain wall orients in the (11) direction of the lattice [9]. After preparing the initial state, the *random-single-spin-flip* Monte Carlo algorithm is performed. We *randomly* select *one spin*, and flip it if the total energy decreases after flipping, and if at least one of the nearest neighbors is already flipped, i.e., only spins at the interface are allowed to flip [25, 26]. A Monte Carlo time step is defined as $L_x \times L_y$ single spin flips. As time evolves, the domain wall propagates and roughens. In Fig. 1, the snapshots of the dynamic evolution of the spin configuration are displayed for different random fields with the uniform distribution. As Δ increases, overhangs first appear then islands.

Due to the existence of the overhangs and islands, there may be different ways to define the domain interface. Here, we adopt the definition with the magnetization.

Denoting a spin at site (x, y) by $S_{xy}(t)$, we introduce a *line* magnetization and height function of the domain interface [12, 13],

$$m(y, t) = \frac{1}{L_x} \left[\sum_{x=1}^{L_x} S_{xy}(t) \right], \quad (3)$$

$$h(y, t) = \frac{L_x}{2} [m(y, t) + 1]. \quad (4)$$

We then calculate the average velocity and roughness function of the domain interface,

$$v(t) = \frac{d\langle h(y, t) \rangle}{dt}, \quad (5)$$

$$\omega^2(t) = \langle h(y, t)^2 \rangle - \langle h(y, t) \rangle^2. \quad (6)$$

Here $\langle \cdot \cdot \cdot \rangle$ represents both the statistical average and the average in y direction.

A more informative quantity is the height correlation function,

$$C(r, t) = \langle [h(y+r, t) - h(y, t)]^2 \rangle. \quad (7)$$

It describes both the spatial correlation of the height function in y direction and the growth of the domain interface in x direction. Further, we consider the Fourier transform of the height function [22, 23],

$$h(k, t) = \frac{1}{\sqrt{L_y}} \sum_{y=1}^{L_y} [h(y, t) - \langle h(y, t) \rangle] \exp(iky). \quad (8)$$

The structure factor is then defined,

$$S(k, t) = \langle h(k, t) h(-k, t) \rangle. \quad (9)$$

To obtain the dynamic exponent z *independently*, we introduce an observable

$$F(t) = [M^{(2)}(t) - M(t)^2] / \omega^2(t). \quad (10)$$

Here $M(t)$ is the global magnetization and $M^{(2)}(t)$ is its second moment. $F(t)$ is nothing but the ratio of the planar susceptibility and line susceptibility.

2.2. Scaling analysis

For the uniform distribution with $\Delta > 1$ and Gaussian distribution of the random fields, the depinning transition is a second-order phase transition. The order parameter, i.e., the average velocity $v(t)$ should obey the dynamic scaling theory supported by the renormalization-group calculations [28, 18, 19]. In the critical regime, there are two spatial length scales in the dynamic relaxation, i.e., the nonequilibrium spatial correlation $\xi(t)$ and the finite lattice size L_y , scaling arguments lead to a dynamic scaling form [28, 18, 19],

$$v(t, \tau, L_y) = b^{-\beta/\nu} G(b^{-z}t, b^{1/\nu}\tau, b^{-1}L_y). \quad (11)$$

Here, b is a rescaling factor, β and ν are the static exponents, z is the dynamic exponent, and $\tau = (H - H_c)/H_c$. Taking $b \sim t^{1/z}$, the dynamic scaling form is rewritten as

$$v(t, \tau, L_y) = t^{-\beta/\nu z} G(1, t^{1/\nu z} \tau, t^{-1/z} L_y). \quad (12)$$

In the short-time regime, i.e., the regime with $\xi(t) \sim t^{1/z} \ll L_y$, the finite-size effect is negligibly small,

$$v(t, \tau) = t^{-\beta/\nu z} G(t^{1/\nu z} \tau). \quad (13)$$

At the depinning transition point $\tau = 0$, a power-law behavior is obtained,

$$v(t) \sim t^{-\beta/\nu z}. \quad (14)$$

With Eq. (13), one may locate the transition field H_c by searching for the best power-law behavior of $v(t, \tau)$ [18, 19]. To determine ν , one simply derives from Eq. (13)

$$\partial_\tau \ln v(t, \tau)|_{\tau=0} \sim t^{1/\nu z}. \quad (15)$$

In general, the roughness function $\omega^2(t)$ and height correlation function $C(r, t)$ may not obey a perfect power-law behavior in early times. Due to the random updating scheme in numerical simulations, the domain interface and its velocity also roughen *even without disorder* ($\Delta = 0$). This leads to rather strong correlations to scaling. To capture the dynamic effects of the disorder, we introduce the pure roughness function

$$D\omega^2(t) = \omega^2(t) - \omega_b^2(t), \quad (16)$$

and height correlation function

$$DC(r, t) = C(r, t) - C_b(r, t), \quad (17)$$

where $\omega_b^2(t)$ and $C_b(r, t)$ are the roughness function and height correlation function for $\Delta = 0$. For a large lattice L_y and at the transition point $H = H_c$, $D\omega^2(t)$ and $DC(r, t)$ should obey the standard power-law scaling behaviors [29, 30, 31, 12],

$$D\omega^2(t) \sim t^{2\zeta/z}, \quad (18)$$

and

$$DC(r, t) \sim \begin{cases} t^{2(\zeta - \zeta_{loc})/z} r^{2\zeta_{loc}} & \text{if } r \ll \xi(t) \ll L_y \\ t^{2\zeta/z} & \text{if } 0 \ll \xi(t) \ll r \end{cases}. \quad (19)$$

Here $\xi(t) \sim t^{1/z}$, ζ is the global roughness exponent, and ζ_{loc} is the local one.

The structure factor should follow a scaling form [22, 23]

$$S(k, t) = k^{-(2\zeta+1)} f_s(kt^{1/z}), \quad (20)$$

where the scaling function takes the form

$$f_s(u) \sim \begin{cases} u^{2(\zeta - \zeta_s)} & \text{if } u \gg 1 \\ u^{2\zeta+1} & \text{if } u \ll 1 \end{cases}, \quad (21)$$

and ζ_s is the *spectral* roughness exponent.

Since $\omega^2(t)$ describes the fluctuation in x direction and $M^{(2)}(t) - M(t)^2$ includes those in both x and y directions, the dynamic exponent z can be determined independently by

$$F(t) \sim \xi(t)/L_y \sim t^{1/z}/L_y. \quad (22)$$

3. Monte Carlo Simulation

We present the results with the random-single-spin-flip Monte Carlo algorithm in the first two subsections, and those with different updating schemes in the third subsection.

3.1. Uniform distribution of random fields

In Fig. 2(a), the interface velocity $v(t)$ is displayed for different driving fields and different strengths of the random fields. For example, at $\Delta = 2.0$, it drops rapidly for smaller H , while approaches a constant for larger H . By searching for the best power-law behavior, one locates the transition fields $H_c = 1.2028(2)$ and $1.4599(2)$ for $\Delta = 1.3$ and 2.0 , respectively. As shown in the figure, $v(t)$ for both $\Delta = 1.3$ and 2.0 at H_c show almost perfect power-law behaviors starting from rather early times. According to Eq. (14), one measures the exponent $\beta/\nu z = 0.244(2)$ and $0.199(2)$ from the slopes of the curves for $\Delta = 1.3$ and 2.0 , respectively.

The transition field H_c varies significantly with the strength of the random fields, as shown in Fig. 2(b), and all the measurements of H_c are summarized in Table 1. The results are qualitatively in agreement with the previous work [24], but with much better accuracy. For $\Delta > 1$, the transition field $H_c < \Delta$, and the depinning transition is of second-order. The order parameter $v(t)$ exhibits a nice power-law behavior, as shown in the Fig. 2(a). For $\Delta \leq 1$, the velocity approaches a constant for $H \geq \Delta$, while drops rapidly to zero once H is slightly smaller than Δ . This is a signal that the depinning transition is of first-order for $\Delta \leq 1$, and the transition field $H_c = \Delta$. Following Fig. 2(b), the transition field H_c increases with Δ , and can be fitted to an exponential function, i.e. $H_c = 1.70 - 2.04 \exp(-1.08\Delta)$.

In Fig. 3(a), the dynamic observable $F(t)$ in Eq. (10) is plotted at H_c . The power-law behavior is detected. According to Eq. (22), $1/z = 0.718(7)$ and $0.788(5)$ are extracted respectively. To calculate the logarithmic derivative $\partial_\tau \ln v(t, \tau) = \partial_\tau v(t, \tau)/v(t, \tau)$, we interpolate $v(t, \tau)$ between different H , e.g., in the interval $[1.195, 1.210]$ for $\Delta = 1.3$, and $[1.456, 1.464]$ for $\Delta = 2.0$. In Fig. 3(b), $\partial_\tau \ln v(t, \tau)$ is plotted at H_c . A power-law behavior is observed. Based on Eq. (15), $1/\nu z = 0.704(6)$ and $0.674(6)$ are derived from the slopes of the curves, respectively.

In Fig. 4(a), the pure roughness function $D\omega^2(t) = \omega^2(t) - \omega_b^2(t)$ is plotted for $\Delta = 1.3$ and 2.0 at the transition field H_c . Here $\omega_b^2(t)$ is the roughness function for $\Delta = 0$. The curves for both $\Delta = 1.3$ and 2.0 show almost perfect power-law behaviors from rather early times. According to Eq. (18), we measure the exponent $2\zeta/z = 1.676(6)$ and $1.665(9)$ from the slopes of the curves respectively.

The structure factor $S(k, t)$ is displayed for $\Delta = 2.0$ at $H_c = 1.4599$ in Fig. 4(b). According to Eq. (21), data collapse for different t is observed in the inset. The exponents used for the data collapse are $\zeta = 1.06$ and $z = 1.27$ obtained from Fig. 3(a) and 4(a) respectively. Obviously, for a small $u = kt^{1/z} \ll 1$, $u^{-(2\zeta+1)} f_s(u)$ approaches a constant. For a large $u \gg 1$, $u^{-(2\zeta+1)} f_s(u)$ exhibits a power-law behavior. One extracts the exponent $2\zeta_s + 1 = 2.68(2)$ from the slope of the curves, i.e., $\zeta_s = 0.84(1)$.

In Fig. 5(a), the pure height correlation function $DC(r, t)$ is displayed for $\Delta = 2.0$ at $H_c = 1.4599$. For a large $r \gg \xi(t)$, e.g., $r = 512$, one extracts the exponent $2\zeta/z = 1.663(4)$ by Eq. (19), consistent with that from Fig. 4(a) within errors. For a small $r \ll \xi(t)$, $DC(r, t)$ should be independent of t for a normal interface with $\zeta = \zeta_{loc}$, according to Eq. (19). But $DC(r, t)$ of $r = 2$ clearly increases with time t . A power-law behavior is observed from rather early times. According to Eq. (19), the slope of the curve gives $2(\zeta - \zeta_{loc})/z = 0.657(4)$. From the measurements of ζ and z from Fig. 3(a) and 4(a), we calculate the local roughness exponent $\zeta_{loc} = 0.643(6)$.

The pure height correlation function $DC(r, t)$ is plotted as a function of r in Fig. 5(b). For a small $r \ll \xi(t)$, there exists a power-law behavior, but this region is rather limited. For a large r , there emerge strong corrections to scaling. We introduce the form of corrections [29],

$$DC(r) \sim [\tanh(r/c)]^{2\zeta_{loc}}. \quad (23)$$

Here, c is an adjustable parameter. The fitting to the curve extends to a larger interval and yields $\zeta_{loc} = 0.645(6)$. It is in agreement with that from Fig. 5(a) within errors.

From the measurements of $\beta/\nu z$, $1/z$, $1/\nu z$, $2\zeta/z$, $2\zeta_s + 1$, $2(\zeta - \zeta_{loc})/z$ and $2\zeta_{loc}$ in Fig. 2 to 5, respectively. We calculate the dynamic critical exponent z , the static critical exponents β and ν , the roughness exponents ζ , ζ_{loc} and ζ_s . All the measurements are summarized in Table 1, compared with those of the QEW equation. In Fig. 6(a), the critical exponents z , ν , and ζ are displayed for different strengths of the random fields. The dynamic critical exponent z decreases with Δ , and the difference between the DRFIM model and QEW equation increases with Δ , up to 20 percent. The critical exponent ν depends non-monotonously on Δ , and the difference between the DRFIM model and QEW equation reaches maximally for $\Delta = 1.3$ and 1.5, over 20 percent. In Fig. 6(b), the critical exponent β decreases monotonously with Δ and reaches constant for $\Delta \geq 1.5$.

In Fig. 7(a), the roughness exponents ζ , ζ_{loc} and ζ_s are plotted for different strengths of the random fields. According to Ref. [22], the exponents ζ , ζ_{loc} and ζ_s are not independent, and there are four different subclasses, namely, Family-Vicsek, super-rough, intrinsic and faceted. Following Fig. 7(a) and Table 1, $\zeta = \zeta_{loc} = \zeta_s$ for $\Delta \leq 1$, and it belongs to the *Family-Vicsek* universality class. In the crossover regime from the first-order transition to the second-order one, e.g., for $\Delta = 1.05$ and 1.1, $\zeta = \zeta_s$, the DRFIM model looks somewhat similar to the QEW equation, but there exists still a major difference, i.e., $\zeta_{loc} < 1$ for the DRFIM model, while $\zeta_{loc} \approx 1$ for the QEW equation. For $\Delta \geq 1.2$, $\zeta \neq \zeta_{loc} \neq \zeta_s$ and $\zeta_{loc} \neq 1$, and it indicates that the DRFIM model belongs to the new universality class suggested in Ref. [23]. Additionally, one interestingly observes that the exponent ζ_s is in agreement with $(\zeta + \zeta_{loc})/2$ within errors. The possible mechanism remains to be understood.

For $\Delta > 1$, the local roughness exponent ζ_{loc} decreases with Δ , and the difference between the DRFIM model and QEW equation increases with Δ , up to over 35 percent. In our opinions, it is mainly the overhangs and islands that induce this difference.

3.2. Gaussian distribution of random fields

As shown in Fig. 2(b), the transition field H_c varies linearly with σ for the Gaussian distribution of the random fields, and all the measurements of H_c are summarized in Table 2. The results are in agreement with those in Ref. [24], but with higher accuracy. Here the depinning transition is always of second-order. The crossover from the second-order phase transition to the first-order one is not present, because the Gaussian distribution is unbounded. All the measurements of the critical exponents are also summarized in Table 2. In Fig. 6(a), variation of the critical exponents z , ν , and ζ with σ for the Gaussian distribution of the random fields is displayed. The dynamic critical exponent z decreases monotonously with σ , similar to that of the uniform distribution of the random fields. However, the static critical exponent ν increases monotonously with σ , different from that of the uniform distribution of the random fields. In our opinions, the non-monotonous behavior of the critical exponents for the uniform distribution of the random fields is induced by the crossover from the second-order transition to the first-order one. In Fig. 7(b), the monotonous decrease of the roughness exponents ζ , ζ_{loc} and ζ_s with σ is displayed for the Gaussian distribution of the random fields. The results indicate $\zeta \neq \zeta_{loc} \neq \zeta_s$ and $\zeta_{loc} \neq 1$, the same as that of the uniform distribution of the random fields.

As shown in Figs. 6 and 7, all the critical exponents z , ν , β , ζ , ζ_{loc} and ζ_s vary in principle with the strength of the random fields, and the dependence of the critical exponents on the strength of the random fields is also different for the uniform and Gaussian distributions. At the limit of the strong random fields, the critical exponents may tend to the same for the uniform and Gaussian distributions, but it is less clear for the roughness exponents ζ_{loc} and ζ_s . In other words, the strong universality is violated in the depinning transition. Both the crossover from the second-order transition to the first-order one in the uniform distribution of the random fields, and the dynamic effect of the overhangs and islands lead to this violation of the universality. It is pointed out in Ref. [13] that overhangs and islands play important roles in the domain-wall motion. As the strength of the random fields changes, the overhangs and islands alter their critical behavior and modify the critical exponents at the depinning transition.

Although the strong universality is violated, we observe that the static exponent β looks somewhat 'universal'. For the Gaussian distribution of the random fields, β is almost independent of the strength of the random fields. For the uniform distribution of the random fields, β also reaches a constant value for $\Delta \geq 1.5$ which coincides with that of the Gaussian distribution. Are there other combinations of the critical exponents which show a 'universal' behavior? In Fig. 6(b), variation of the exponents $(2\zeta+1)/z$ and $\beta/\nu z$ with the strength of the random fields is displayed. In particular, the exponent $(2\zeta+1)/z$ looks 'universal', similar to the exponent β . According to Eqs. (18) and (22), $M^{(2)}(t) - M(t)^2 \sim t^{(2\zeta+1)/2}$. In other words, the scaling exponent of the *planar* susceptibility is 'universal'. Since $M(t)$ is equivalent to the average height function, $M^{(2)}(t) - M(t)^2$ is nothing but the fluctuation of the domain wall.

3.3. Updating schemes

To further understand the universality at the depinning transition, we examine different update schemes in the Monte Carlo simulations, e.g., the sequential sweep and parallel sweep. For the *sequential* sweep, we select a spin sequentially by the row perpendicular to the domain wall, and flip it if the total energy decreases after flipping. For the *parallel* sweep, we divide the lattice into two 'checkerboard' sublattices. The spins in each sublattice do not directly interact each other. Therefore we may update all the spins in each sublattice simultaneously. Different updating schemes in the Monte Carlo algorithm do not modify the transition field and critical exponents, and all the measurements are summarized in Table 3. The small deviation in the transition field H_c and the exponent β should be induced by corrections to scaling in the early times.

Because of the presence of the random fields, the magnetic system has many local minima separated by sizeable energy barriers. During the dynamic evolution, the system may be trapped in a local minimum without finding the global one, as a consequence, remains far from equilibrium. The lifetime of a metastable state may be considered as infinite at zero-temperature. This type of behavior is well modeled by the single-spin-flip Monte Carlo dynamics [27]. In order to verify the reliability of the single-spin-flip Monte Carlo dynamics, the two-spin-flip algorithm has been also performed. The power-law behaviors in Fig 2 to 5 are observed. All the measurements of the depinning transition field and critical exponents are summarized in Table 3. The depinning transition field H_c is changed, but all the exponents are in agreement within errors with those of the single-spin-flip dynamics [27].

4. Conclusion

With Monte Carlo methods, we have simulated the dynamic relaxation of a domain wall in the two-dimensional DRFIM model. Based on the short-time dynamic scaling forms, the transition field and all critical exponents at the depinning transition are accurately determined. Since the measurements are carried out at the beginning of the time evolution, the dynamic approach does not suffer from critical slowing down.

The results are first presented for the uniform distribution of the random fields with the single-spin-flip Monte Carlo dynamics.

i) For $\Delta \leq 1$, the depinning transition is of first-order, and the transition field $H_c = \Delta$. The exponents β and ν do not exist, but the growth dynamics of the domain wall is still meaningful. Since $\zeta = \zeta_{loc} = \zeta_s$, it belongs to the *Family-Vicsek* universality class.

ii) For $\Delta > 1$, the depinning transition is of second-order, and the transition field $H_c < \Delta$. As shown in Fig. 6(a) and Fig. 7(a), critical exponents vary significantly with Δ . Except for the dynamic exponent z , all other critical exponents indicate the crossover from the first-order transition to the second-order one. The exponent ν and roughness exponents exhibit non-monotonous dependence on Δ .

iii) For $\Delta > 1$ and $\Delta \rightarrow 1$, e.g., at $\Delta = 1.05$ and 1.1 , the DRFIM model looks somewhat similar to the QEW equation, but $\zeta_{loc} \neq 1$. If $\zeta_{loc} = 1$, it would be in the so-called *super-rough* universality class as the QEW equation is. For $\Delta \geq 1.2$, one observes clearly $\zeta \neq \zeta_{loc} \neq \zeta_s$, and $\zeta_{loc} < 1$. It indicates that the DRFIM model belongs to the new dynamic universality class suggested in Ref. [23].

For comparison, simulations have been also performed for the Gaussian distribution of the random fields. The crossover from the second-order transition to the first-order one is not present in this case. Generally speaking, the strong universality is violated in the depinning transition, and the critical exponents vary significantly with the strength and form of the random fields. In our opinion, the difference between the uniform and Gaussian distributions of the random fields is mainly induced by the crossover from the second-order transition to the first-order one in the former case, and the dependence of the critical exponents on the strength of the random fields comes also from the overhangs and islands. Finally, our simulations confirm that the critical exponents are independent of the updating schemes.

Acknowledgments

This work was supported in part by NNSF of China under Grant Nos. 10875102 and 11075137, and Research Projects of Education Department of Zhejiang No. Y200803742.

References

- [1] Nattermann T, Pokrovsky V and Vinokur V M 2001 *Phys. Rev. Lett.* **87** 197005
- [2] Glatz A, Nattermann T and Pokrovsky V 2003 *Phys. Rev. Lett.* **90** 047201
- [3] Rosso A, Hartmann A K and Krauth W 2003 *Phys. Rev. E* **67** 021602
- [4] Duemmer O and Krauth W 2005 *Phys. Rev. E* **71** 061601
- [5] Kolton A B, Rosso A, Albano E V and Giamarchi T 2006 *Phys. Rev. B* **74** 140201(R)
- [6] Kolton A B, Rosso A, Giamarchi T and Krauth W 2006 *Phys. Rev. Lett.* **97** 057001
- [7] Kleemann W 2007 *Annu. Rev. Mater. Res.* **37** 415
- [8] Bustingorry S, Kolton A B and Giamarchi T 2008 *Europhys. Lett.* **81** 26005
- [9] Nowak U and Usadel K D 1998 *Europhys. Lett.* **44** 634
- [10] Roters L, Hucht A, Lübeck S, Nowak U and Usadel K D 1999 *Phys. Rev. E* **60** 5202
- [11] Roters L, Lübeck S and Usadel K D 2001 *Phys. Rev. E* **63** 026113
- [12] Zhou N J, Zheng B and He Y Y 2009 *Phys. Rev. B* **80** 134425
- [13] Zhou N J and Zheng B 2010 *Phys. Rev. E* **82** 031139
- [14] Metaxas P J, Jamet J P and Mougín A *et al* 2007 *Phys. Rev. Lett.* **99** 217208
- [15] Lemerle S, Ferré J and Chappert C *et al* 1998 *Phys. Rev. Lett.* **80** 849
- [16] Jost M, HeimeI J and Kleinefeld T 1998 *Phys. Rev. B* **57** 5316
- [17] Rosso A and Krauth W 2001 *Phys. Rev. Lett.* **87** 187002
- [18] Zheng B 1998 *Int. J. Mod. Phys. B* **12** 1419 (review article)
- [19] Luo H J, Schülke L and Zheng B 1998 *Phys. Rev. Lett.* **81** 180
- [20] Rodríguez-Rodríguez G and Pérez-Junquera A *et al* 2007 *J. Phys. D: Appl. Phys.* **40** 3051
- [21] Kolton A B, Schehr G and Le Doussal P 2009 *Phys. Rev. Lett.* **103** 160602
- [22] Ramasco J J, López J M and Rodríguez M A 2000 *Phys. Rev. Lett.* **84** 2199
- [23] Chen Y J, Nagamine Y, Yamaguchi T and Yoshikawa K 2010 *Phys. Rev. E* **82** 021604
- [24] Ji H and Robbins M O 1991 *Phys. Rev. A* **44** 2538

- [25] Koiller B and Robbins M O 2010 *Phys. Rev. B* **82** 064202
 [26] Drossel B and Dahmen K 1998 *Eur. Phys. J. B* **3** 485
 [27] Vives E, Rosinberg M L and Tarjus G 2005 *Phys. Rev. B* **71** 134424
 [28] Janssen H K, Schaub B and Schmittmann B 1989 *Z. Phys. B* **73** 539
 [29] Jost M and Usadel K D 1996 *Phys. Rev. B* **54** 9314
 [30] Zhou N J and Zheng B 2008 *Phys. Rev. E* **77** 051104
 [31] Bakó B, Weygand D, Samaras M, Hoffelner W and Zaiser M 2008 *Phys. Rev. B* **78** 144104

Δ	$v(t)$			$F(t), C(r, t)$	$\omega^2(t), C(r, t)$	$C(r, t)$	$S(k, t)$
	H_c	β	ν	z	ζ	ζ_{loc}	ζ_s
≤ 1.0	Δ			1.50(1)	0.49(1)	0.48(2)	0.49(1)
1.05	1.0447(1)	0.621(8)	1.35(3)	1.49(1)	1.00(1)	0.86(1)	1.02(2)
1.1	1.0833(2)	0.411(4)	1.12(2)	1.46(1)	1.10(1)	0.83(1)	1.10(1)
1.2	1.1485(2)	0.388(3)	1.08(2)	1.44(1)	1.19(1)	0.80(1)	1.01(1)
1.3	1.2028(2)	0.347(3)	1.02(2)	1.39(1)	1.17(1)	0.78(1)	0.99(1)
1.5	1.2933(2)	0.295(3)	1.02(3)	1.33(1)	1.14(1)	0.74(1)	0.94(1)
1.7	1.3670(2)	0.296(3)	1.10(2)	1.30(1)	1.10(1)	0.69(1)	0.91(1)
2.0	1.4599(2)	0.295(3)	1.17(2)	1.27(1)	1.06(1)	0.65(1)	0.84(1)
2.3	1.5398(2)	0.299(3)	1.21(2)	1.26(1)	1.04(1)	0.61(1)	0.82(1)
QEW		0.33(2)	1.33(4)	1.50(3)	1.25(1)	0.98(6)	1.25(1)

Table 1. The depinning transition field and critical exponents obtained for different strengths of the random fields with the uniform distribution are compared with those of the QEW equation in Refs. [4, 5, 8].

σ	$v(t)$			$F(t), C(r, t)$	$\omega^2(t), C(r, t)$	$C(r, t)$	$S(k, t)$
	H_c	β	ν	z	ζ	ζ_{loc}	ζ_s
0.8	1.3607(3)	0.334(3)	1.07(2)	1.36(1)	1.15(1)	0.75(1)	1.03(1)
1.0	1.4205(3)	0.306(3)	1.09(2)	1.34(1)	1.14(1)	0.73(1)	0.94(1)
1.2	1.4779(3)	0.293(3)	1.11(2)	1.31(1)	1.10(1)	0.68(1)	0.91(1)
1.4	1.5355(3)	0.291(3)	1.15(2)	1.29(1)	1.07(1)	0.64(1)	0.89(1)
1.8	1.6505(3)	0.296(3)	1.17(2)	1.27(1)	1.04(1)	0.59(1)	0.78(1)
2.2	1.7647(3)	0.295(3)	1.19(2)	1.24(1)	1.00(1)	0.54(1)	0.70(1)

Table 2. The depinning transition field and critical exponents for the Gaussian distribution of the random fields.

	sweep	H_c	β	ν	z	ζ	ζ_{loc}	ζ_s
SSF	random	1.2028(2)	0.347(3)	1.02(2)	1.39(1)	1.17(1)	0.78(1)	0.99(1)
	sequential	1.2034(4)	0.345(6)	1.02(2)	1.40(1)	1.17(1)	0.77(1)	0.99(1)
	parallel	1.2033(4)	0.338(6)	1.00(2)	1.40(1)	1.17(1)	0.77(1)	0.99(1)
TSF	random	0.7545(3)	0.340(6)	1.01(2)	1.40(2)	1.19(2)	0.78(2)	1.01(2)

Table 3. The depinning transition field and critical exponents for the uniform distribution of the random fields at $\Delta = 1.3$ with different update schemes. SSF: the single-spin-flip; TSF: the two-spin-flip.

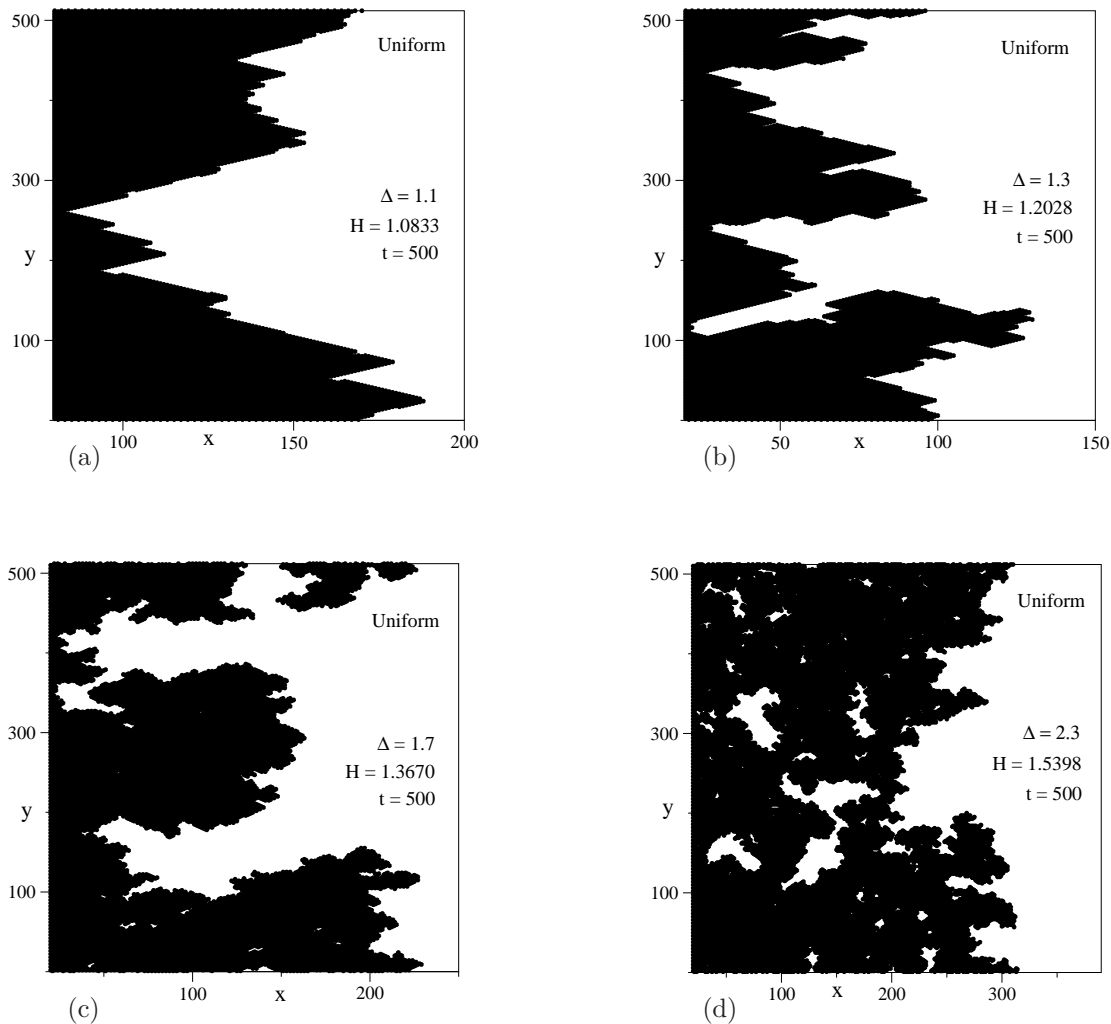


Figure 1. Snapshots of the spin configuration for the uniform distribution of the random fields. The black denotes the spin $S_i = 1$ and the white denotes the spin $S_i = -1$. Simulations are performed with the random-single-spin-flip Monte Carlo algorithm.

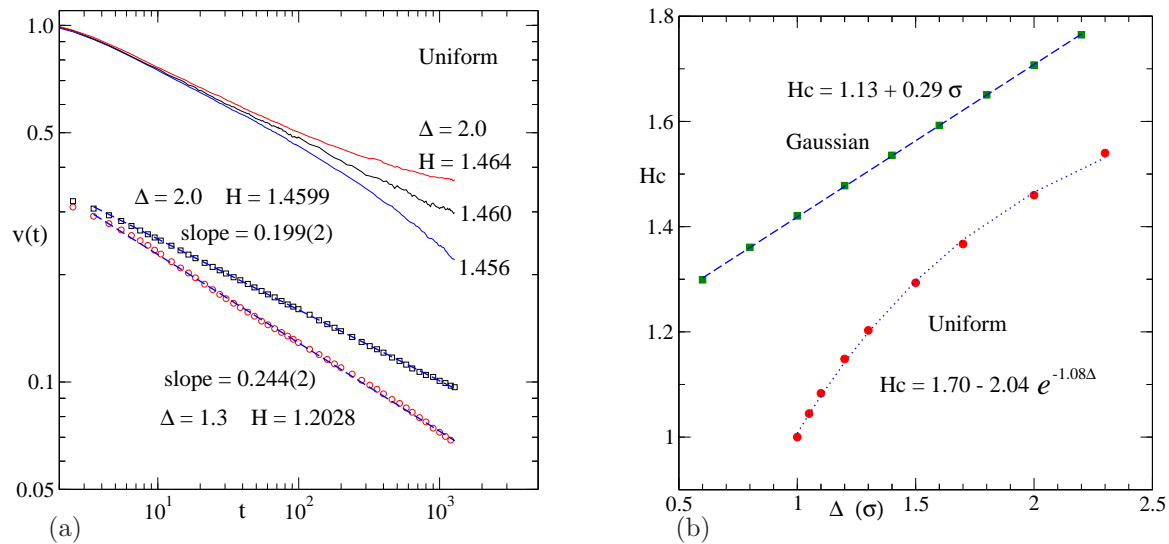


Figure 2. (a) Interface velocity $v(t)$ is displayed for different driving fields H at $\Delta = 2.0$ with solid lines for the uniform distribution of the random fields. For comparison, $v(t)$ is also plotted for $\Delta = 1.3$ and 2.0 at $H_c = 1.2028$ and 1.4599 respectively with circles and squares. Dashed lines show power-law fits. For clarity, the solid lines are shifted up. (b) The transition field H_c is displayed, with Δ and σ for the uniform and Gaussian distributions of the random fields respectively. The dotted and dashed lines show exponential and linear fits respectively. Errors are smaller than the symbol sizes.

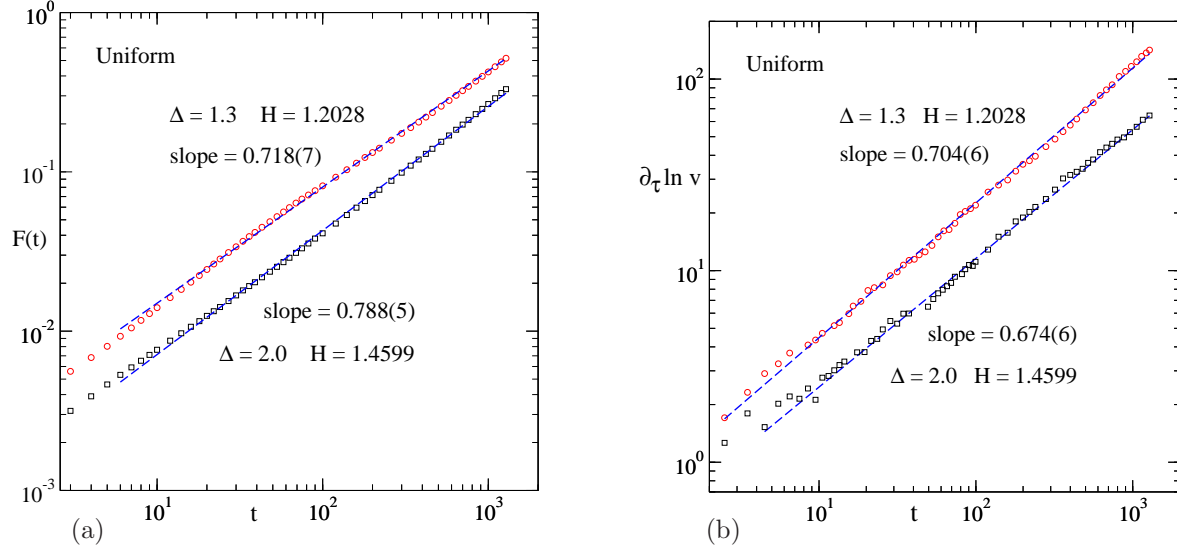


Figure 3. (a) $F(t)$ is plotted for $\Delta = 1.3$ and 2.0 at H_c . For clarity, the curve for $\Delta = 1.3$ is shifted up. (b) The logarithmic derivative of $v(t, \tau)$ is plotted for $\Delta = 1.3$ and 2.0 at H_c . In both (a) and (b), the results are for the uniform distribution of the random fields, and dashed lines show power-law fits.

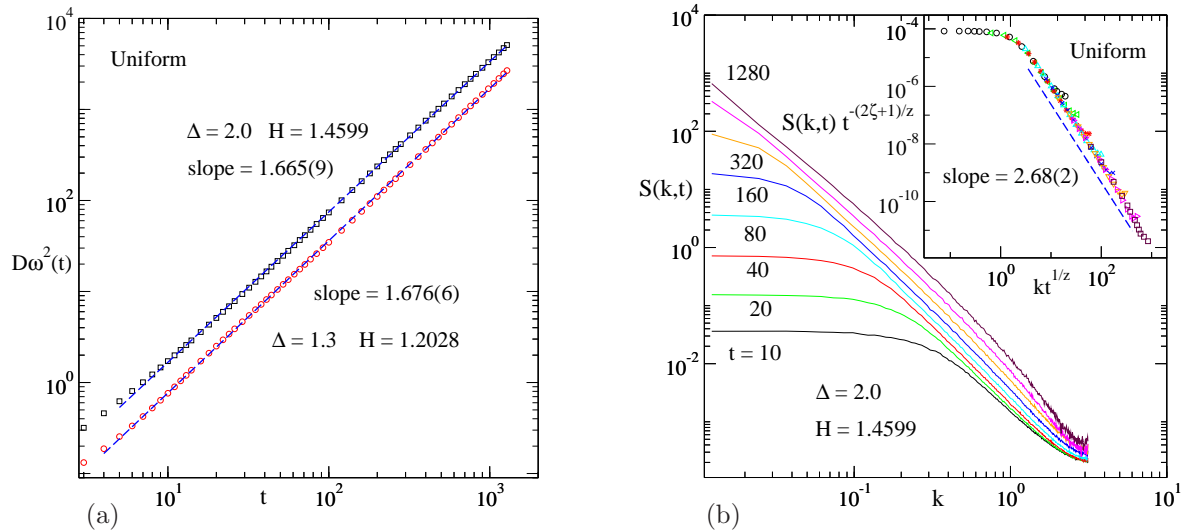


Figure 4. (a) The pure roughness function $D\omega^2(t)$ is displayed for $\Delta = 1.3$ and 2.0 at H_c . (b) The structure factor $S(k, t)$ is plotted for $\Delta = 2.0$ at H_c . In the inset, data collapse for different t is shown. In both (a) and (b), the results are for the uniform distribution of the random fields, and dashed lines show power-law fits.

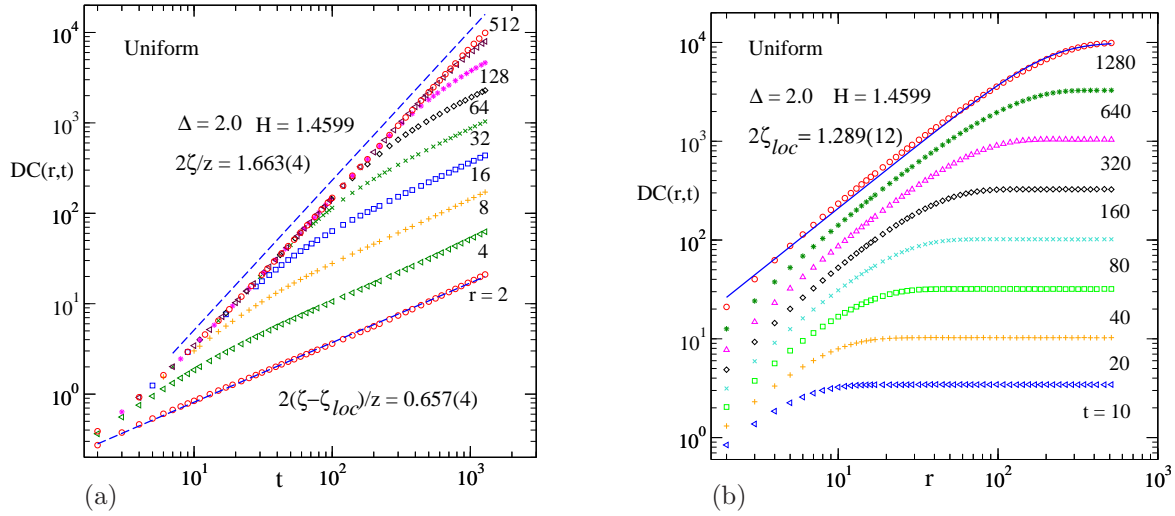


Figure 5. (a) Time evolution of the pure height correlation function $DC(r, t)$ is displayed for $\Delta = 2.0$ at H_c . Dashed lines show power-law fits. (b) $DC(r, t)$ is plotted as a function of r for $\Delta = 2.0$ at H_c . The solid line shows a power-law fit with a hyperbolic tangent correction. In both (a) and (b), the results are for the uniform distribution of the random fields.

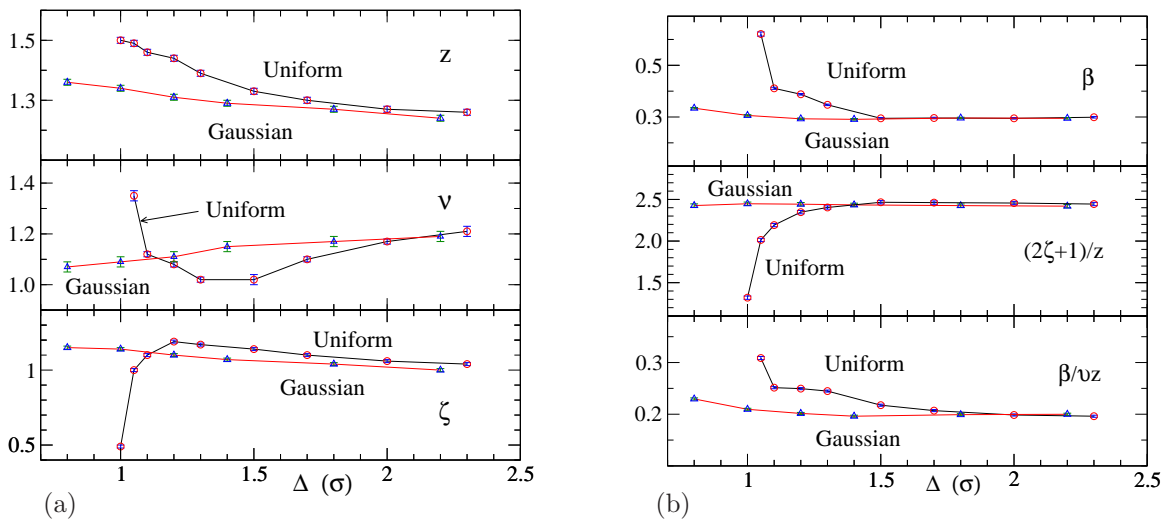


Figure 6. In (a) and (b), variation of the critical exponents z , ν , ζ , β , $(2\zeta + 1)/z$ and $\beta/\nu z$ with Δ and σ respectively for the uniform and Gaussian distributions of the random fields is displayed.

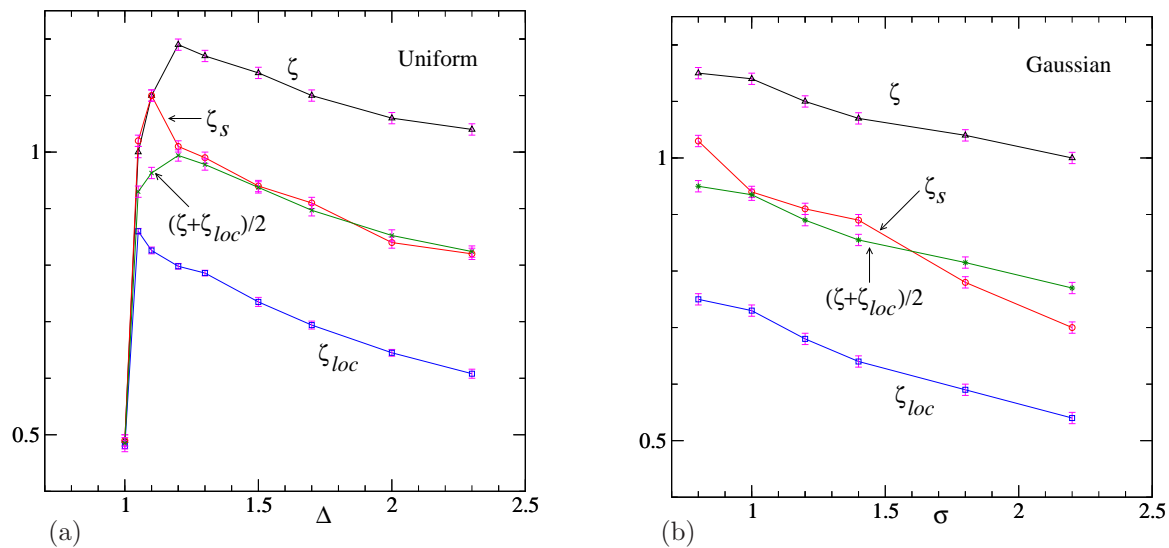


Figure 7. (a) The roughness exponents ζ , ζ_{loc} , ζ_s and $(\zeta + \zeta_{loc})/2$ are plotted for the uniform distribution of the random fields. (b) The roughness exponents ζ , ζ_{loc} , ζ_s and $(\zeta + \zeta_{loc})/2$ are displayed for the Gaussian distribution of the random fields. In both (a) and (b), full lines are just to guide the eyes.